AIP | Physics of Plasmas

Delineating the magnetic field line escape pattern and stickiness in a poloidally diverted tokamak

Caroline G. L. Martins, M. Roberto, and I. L. Caldas

Citation: Physics of Plasmas (1994-present) **21**, 082506 (2014); doi: 10.1063/1.4892395
View online: http://dx.doi.org/10.1063/1.4892395
View Table of Contents: http://scitation.aip.org/content/aip/journal/pop/21/8?ver=pdfcov
Published by the AIP Publishing

Delineating the magnetic field line escape pattern and stickiness in a poloidally diverted tokamak

Caroline G. L. Martins,[1,2,a)] M. Roberto,[1,b)] and I. L. Caldas[3,a)]
[1]*Departamento de Física, Instituto Tecnológico de Aeronáutica, São José dos Campos, SP 12228-900, Brazil*
[2]*Department of Physics, Institute for Fusion Studies, University of Texas at Austin, Austin, Texas 78712, USA*
[3]*Universidade de São Paulo, Instituto de Física, São Paulo, SP 05315-970, Brazil*

(Received 30 October 2013; accepted 25 July 2014; published online 6 August 2014)

We analyze a Hamiltonian model with five wire loops that delineates magnetic surfaces of tokamaks with poloidal divertor. Non-axisymmetric magnetic perturbations are added by external coils, similar to the correction coils that have been installed or designed in present tokamaks. To show the influence of magnetic perturbations on the field line escape, we integrate numerically the field line differential equations and obtain the footprints and deposition patterns on the divertor plate. Moreover, we show that the homoclinic tangle describes the deposition patterns in the divertor plate, agreeing with results observed in sophisticated simulation codes. Additionally, we show that while chaotic lines escape to the divertor plates, some of them are trapped, for many toroidal turns, in complex structures around magnetic islands, embedded in the chaotic region, giving rise to stickiness evidences characteristic of chaotic Hamiltonian systems. Finally, we introduce a random collisional term to the field line mapping to investigate stickiness alterations due to particle collisions. Within this model, we conclude that, even reduced by collisions, the observed trapping still influences the field line transport. The results obtained for our numerical estimations indicate that the reported trapping may affect the transport in present tokamaks. © *2014 AIP Publishing LLC*.
[http://dx.doi.org/10.1063/1.4892395]

I. INTRODUCTION

In conventional tokamaks the plasma column is separated from the wall by a physical limiter made of a material that resists the impact and the temperature of plasma particles.[1] An alternative separation of the plasma column and the chamber's wall can be achieved installing poloidal divertors.

Divertors are essential components in modern tokamaks, such as ITER,[2] and they consist of conductors arranged externally, that carry electric currents in the same direction of the plasma current, in the toroidal direction of the tokamak. A X point (or hyperbolic fixed point) will appear at the positions where the poloidal magnetic field is null, due to the overlap of the magnetic fields of the conductors with the magnetic field of the plasma. From the X point arises a separatrix with two manifolds, one stable and another unstable. Outside the separatrix the surfaces intersect the collector plates, which play a role similar to the physical limiter in conventional tokamaks.[3,4]

Numerical equilibria reconstructions to simulate plasmas in the presence of poloidal divertors are well known in the literature.[5] However, the computation to integrate magnetic field lines, for such magnetic configuration, is time-consuming.[6–8] On the other hand, simple models can delineate quite well dynamical properties of open and closed fields lines near the separatrix. In particular, a simple way to delineate the MHD equilibrium magnetic field in tokamaks is to consider the magnetic configuration created by a set of coils or wires.[9,10]

Wires carrying electric current generate concentric circles of magnetic field lines around themselves. If another wire is positioned parallel to the first one, magnetic field lines are no longer circular, although they are still closed curves around each wire. For such magnetic configuration, there will be a point where the magnetic field is zero. In this position arise two manifolds of the separatrix, forming a X point. A large number of wires distort the magnetic fields, creating more than one X point and their respective separatrixes.

Non-axisymmetric magnetic perturbations destroy the magnetic separatrix creating homoclinic tangles, leading to the formation of a layer of chaotic field lines.[5,11] Due to the flexibility of models based on magnetic fields produced by wires, one can consider different effects by adequately specifying the perturbations. Thus, perturbed wire models have been used to analyze a range of dynamical properties in double-null (two X-points) and single-null (one X-point) diverted tokamaks, such as, the width of the scrape-off layer,[12] chaotic layer formation,[13–15] and particle drift orbits.[16]

A model described by five parallel infinite wires was analyzed in Ref. 9, to simulate the magnetic surfaces of diverted tokamaks, in the presence of magnetic perturbations created by error fields due to asymmetries on the external coils.[13,17] Moreover, a Hamiltonian with three loop wires was analyzed in Ref. 10, to describe two mapping methods and to study the stochastic field lines in poloidal divertor tokamak plasmas affected by external non-axisymmetric magnetic perturbations.

Following Ref. 10, in the present work we analyze a Hamiltonian model with five loop wires that enables the

[a)]Electronic addresses: carolinegameiro@gmail.com and ibere@if.usp.br
[b)]Author to whom correspondence should be addressed. Electronic mail: marisar@ita.br

choice of magnetic axis position, triangularity, and elongation. The versatility of the model allows us to delineate equilibrium magnetic surfaces that reproduce ITER like magnetic topology, including a similar safety factor profile. Here, we add to equilibrium perturbations created by pairs of loop coils carrying opposite flowing currents, introduced in Ref. 10. Those perturbations are similar to the ones related to the correction coils (C-coils) installed at the DIII-D tokamak[5] and those that will be installed at ITER.[18]

Thus, using the mentioned Hamiltonian description we solve numerically the perturbed magnetic field line differential equations and show the influence of magnetic perturbations on the deposition patterns at the divertor plate. To do that, we calculate the numbers of toroidal turns, called connection lengths, performed by the perturbed magnetic field lines until reaching the divertor plates and their non uniform distribution, the deposition patterns, on the divertor plates.[5,6,11] Moreover, we show that the homoclinic tangle describes the deposition patterns in the divertor plate, agreeing with results observed in sophisticated simulation codes.[19,20] Additionally, we show that even so the chaotic lines escape to the divertor plates, some of them are trapped, for many toroidal turns, in complex structures around magnetic islands, embedded in the chaotic region, giving rise to the so called stickiness effect characteristic of Hamiltonian systems.[21] So, our results indicate that the deposition on the plates depends on the sticky structure of the analyzed magnetic configuration. Finally, we introduce a random collisional term to the field line mapping to reproduce stickiness alterations due to particle collisions. Within this model, we conclude that, even reduced by collisions, stickiness still influences the field line transport.

In Sec. II, we introduce the equilibrium magnetic surfaces of our five loop wires model. In Sec. III, we present the resonant perturbation caused by external loop coils. Numerical results on homoclinic tangle formation and examples of escape pattern typical of those computed for tokamaks are presented in Sec. IV. Stickiness effect investigations are in Sec. V, and its alterations due to particle collisions in Sec. VI; finally, in Sec. VII we present the conclusions.

II. EQUILIBRIUM MODEL

To describe the equilibrium magnetic field lines, we choose a coordinate system appropriated to the tokamak symmetry, shown in Figure 1.

We will consider in this work a simple model that consists of five wire loops carrying electric currents, with the same relative position proposed in Ref. 9, as shown in Table I.

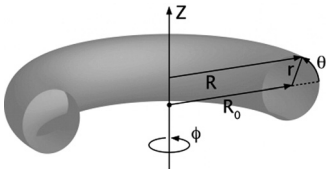

FIG. 1. Geometry of a toroidal system.

As introduced in the Appendix, for a tokamak with large aspect ratio, $(R_0/a \gg 1)$, the unperturbed Hamiltonian, can be approximated to

$$H_0(z,p_Z) = \frac{-1}{R_0}\sum_{j=1}^{5}\frac{\mu_0 I_j}{4\pi B_0}\left(\ln\left(64\left(\left[\left(\frac{R}{R_0}-\frac{R_j}{R_0}\right)^2 + \left(\frac{Z}{R_0}-\frac{Z_j}{R_0}\right)^2\right]^{-1}\right)\right) - 4\right). \quad (1)$$

The wire 1 represents the plasma current. The role of the wires 2 and 3 is to create the lower and upper X points, respectively. These two X points are located in distinct separatrices: the active separatrix (internal) and the inactive separatrix (external). The outer separatrix is called inactive because the plasma does not reach this position; on the other hand, it plays an important role in the shape of the surfaces. The negative currents in wires 4 and 5 compress the left and right sides of the magnetic surfaces, then one can model the desired elongation of the plasma column.

Figure 2(a) shows the positions of the intersections of the five loops with the R-Z plane and the surfaces generated by them. Figure 2(b) shows the surfaces related to the plasma column and two X points: the upper X point of the external separatrix (inactive), and the lower X point of the internal separatrix (active), that defines the boundary of the plasma.

Each magnetic surface has a well-defined characteristic known as rotation number, which is the average of the poloidal angle performed by a field line after a full toroidal turn. In this model, the poloidal angle is the angular displacement in the plane R-Z made by a field line. For tokamaks, the inverse of the rotational number is the safety factor, and it is used to characterize the topology of the lines.

In order to obtain the safety factor profile of the magnetic surfaces, we integrate the unperturbed magnetic field lines equations (see Appendix A) for many initial conditions located on a horizontal line, indicated in Figure 2(b). We consider that a field line completes m toroidal turns if $\varphi = 2m\pi R_0$. Thus, on rational surfaces with safety factor $q = m/n$, the periodic field lines perform m toroidal turns and n poloidal turns.

Figure 3 shows the safety factor profile calculated from our model, for initial conditions located at the auxiliary line of Figure 2(b). In this figure, it is possible to identify the positions of two surfaces with infinite safety factor. These surfaces correspond to the two separatrixes shown in Figure 2(b). In a magnetic system, hyperbolic points correspond to the positions with null poloidal magnetic field and, consequently, the values of the safety factor goes to infinity.

TABLE I. Wires positions and currents values.

n	R_n (m)	Z_n (m)	I_n (MA)
1 (plasma)	6.41	0.513	15.00
2	3.72	−7.580	15.90
3	3.20	8.600	16.28
4	2.45	0.513	−5.69
5	10.00	0.513	−4.60

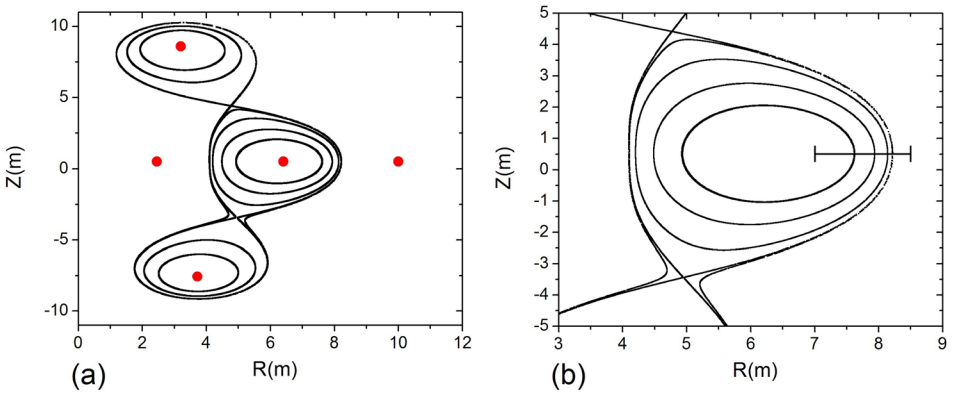

FIG. 2. (a) Magnetic surfaces. The red dots represent the intersection of the five loops with the plane R-Z. (b) Zoom in (a) showing the plasma column, and the upper and lower X points, forming the outer separatrix (inactive) and the inner separatrix (active), respectively. The auxiliary line indicates the initial conditions to calculate the safety factor of Figure 3.

Profiles similar to that shown in Figure 3 are expected for present tokamaks.[22]

III. PERTURBED MODEL BY EXTERNAL COILS

Many tokamaks have non-axisymmetric perturbation coils designed specifically to create chaotic layers in the peripheral region of the plasma column.[23–25] Despite this, few theoretical or experimental data may be found to understand the effects of these chaotic layers in plasmas with elongation and triangularity in the presence of poloidal divertors.

In this work, we consider a non-axisymmetric perturbation generated by $N = 10$ pairs of loop coils carrying opposite currents, $\pm I_c$, positioned at $(R_{c+}, Z_{c+}) = (10.2, 3)$ and $(R_{c-}, Z_{c-}) = (10.2, -3)$. The perturbation created by these coils is similar to the correction coils (C-coils) installed at the DIII-D tokamak,[5] and those that will be installed at ITER.[18] An illustration of this design can be seen in Figure 4, which shows the transversal cross section of the tokamak equilibrium, and ten pairs of coils arranged around the chamber.

For a large aspect ratio tokamak, the perturbing Hamiltonian, $H_1(z, p_Z, \varphi)$, related to the scheme shown in Figure 4, can be approximated by[10]

$$\varepsilon H_1(z, p_Z, \varphi) = \frac{\mu_0 I_c(\varphi)}{4\pi B_0 R_0}\left(\ln\left(\left(\frac{R - R_{c+}}{R_0}\right)^2 + \left(\frac{Z - Z_{c+}}{R_0}\right)^2\right) - \ln\left(\left(\frac{R - R_{c-}}{R_0}\right)^2 + \left(\frac{Z - Z_{c-}}{R_0}\right)^2\right)\right), \quad (2)$$

where the current in the coils, $I_c(\varphi)$, is periodically changing along the toroidal angle, φ, and can be represented by the discontinuity function, $I_c(\varphi) = (-1)^k I_c$, for $(\pi/N)k < \varphi < (\pi/N)(k+1)$ and $k = 0, \ldots, (2N-1)$. This function can be expanded in Fourier series[10]

$$I_c(\varphi) = \frac{4I_c}{\pi}\sum_{p=0}^{\infty}\frac{\sin[(2p+1)N\varphi]}{2p+1}. \quad (3)$$

We will consider only the first term, $p = 0$, of the function (3), since this term gives the main effect of the perturbation. The contribution of higher order toroidal modes, $(2p+1)N$, decreases exponentially while increasing p.[10] Therefore, the perturbing Hamiltonian is reduced to

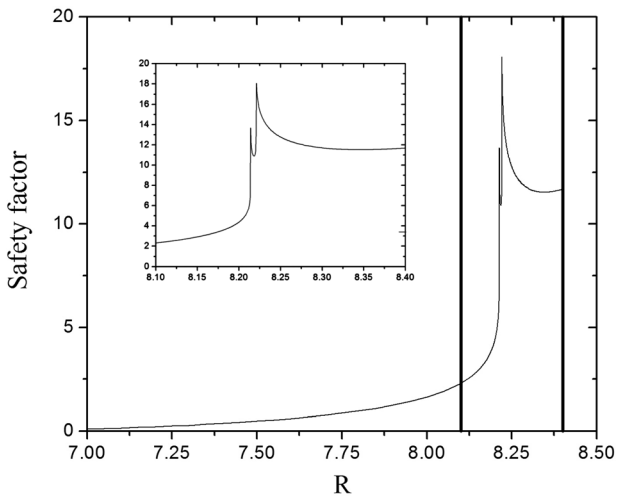

FIG. 3. Safety factor profile for initial conditions located at the auxiliary line from figure 2(b). The rectangle indicates the region amplified. The two points where the safety factor values go to infinity represent the two separatrixes formed by the lower and upper X points.

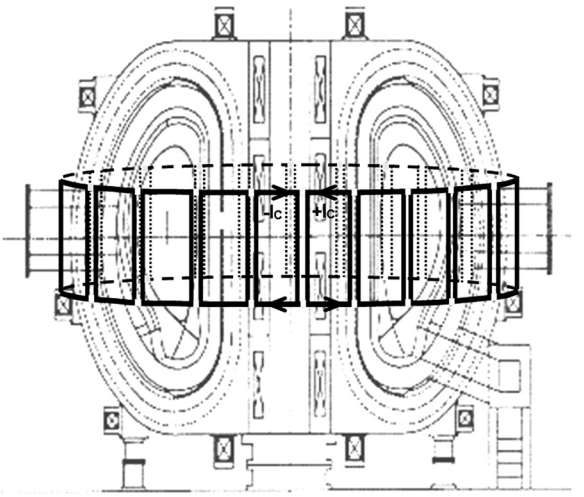

FIG. 4. Transversal cross section of the tokamak ITER with the addition of $N = 10$ pairs of perturbation coils located on the equatorial plane of the chamber, carrying opposing currents, $\pm I_c$, at positions $(R_{c+}, Z_{c+}) = (10.2, 3)$ and $(R_{c-}, Z_{c-}) = (10.2, -3)$.

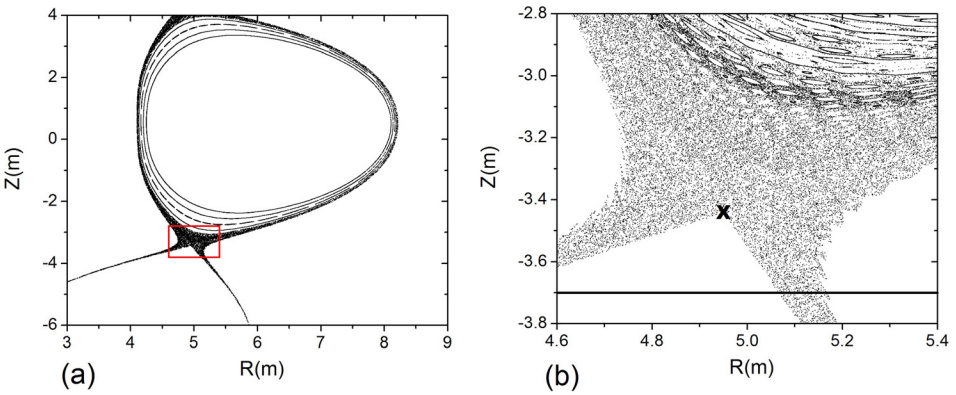

FIG. 5. (a) Magnetic surfaces perturbed by $N = 10$ pairs of loop coils with $I_c = 70\,\text{kA}$. (b) Zoom in (a) showing some islands immersed in the chaotic region. The solid lined segment represents the divertor plate. The black X shows the position of the hyperbolic fixed point.

$$\varepsilon H_1(z,p_Z,\varphi) = \varepsilon\frac{\mu_0 I_p}{\pi^2 B_0 R_0}\left(\ln\left(\left(\frac{R-R_{c+}}{R_0}\right)^2+\left(\frac{Z-Z_{c+}}{R_0}\right)^2\right)\right.$$
$$\left.-\ln\left(\left(\frac{R-R_{c-}}{R_0}\right)^2+\left(\frac{Z-Z_{c-}}{R_0}\right)^2\right)\right)\sin[N\varphi], \tag{4}$$

where the perturbation parameter is $\varepsilon = (I_c/I_p)$.[10]

The total Hamiltonian in canonical coordinates of position and momentum is given by

$$H(z,p_Z,\varphi) = H_0(z,p_Z) + \varepsilon H_1(z,p_Z,\varphi). \tag{5}$$

The set of equations

$$\frac{dz}{d\varphi} = \frac{\partial H}{\partial p_Z}, \quad \frac{dp_Z}{d\varphi} = -\frac{\partial H}{\partial z} \tag{6}$$

was numerically integrated with perturbation parameter $\varepsilon \cong 0.0047$ that corresponds to $I_c = 70\text{kA}$. The value used for the current in the coils was deducted from Ref. 5, which shows the range of the current amplitude applied in the correction coils (C-coil) installed at the DIII-D tokamak, which is, approximately, 0.266%–0.533% of the plasma current. By the same consideration, we define a limit range for the current in our perturbation coils as that expected for ITER tokamak, which is therefore, $I_c = 40\,\text{kA}$ to $I_c = 80\,\text{kA}$.

Figures 5(a) and 5(b) show a chaotic layer around the lower hyperbolic point. The magnetic field lines are no longer closed, and, eventually, reach the divertor plates located horizontally at $Z = -3.7\,\text{m}$ (represented by the black segment in Figure 5(b)), following the manifolds that leave the X point. One can notice, in Figure 5(b), magnetic islands immersed in the chaotic layer, which play an important role in the field lines escape.[26]

IV. HOMOCLINIC TANGLE AND ESCAPE PATTERNS

Since the topology of the manifolds is highly unstable and can be destroyed by arbitrary perturbations,[11,27] it is essential to study the behavior of the field lines near the separatrix and particularly around the X point, to understand the way in which particles are transported through the separatrix.[28,29]

Accordingly, we consider our model to calculate the escape of the field lines to the divertor plates, placed horizontally at $Z = -3.7\,\text{m}$ (black segment in Figure 5(b)). As the particles follow the field lines, the structure of escape obtained must be closely related to measurable profiles of particle deposition on the divertor plates.[5] To analyze the escape of the field lines in question, we calculated the connection length, which is the number of toroidal turns performed by a field line until it reaches the plate. The field line is integrated forward and backward in φ, for initial conditions in a box with $4.88 \leq R_0 \leq 5.02$ and $-3.50 \leq Z_0 \leq -3.35$. Then, a color map is constructed where the color indicates the number of toroidal turns that the field line needs to reach the plate, and the axes, (R, Z), represent the initial position of the field lines.

The manifolds of Figure 6(a) were approximated by numerically integrating initial conditions in a small grid constructed around the hyperbolic fixed point ($R \approx 4.9506\,\text{m}$, $Z \approx -3.4428\,\text{m}$). Figure 6(a) shows the stable (blue) and unstable (red) manifolds of the lower hyperbolic fixed point (in black) for system perturbed by $N = 10$ pairs of loop coils with $I_c = 70\,\text{kA}$. Each individual manifold does not intersect itself, but the two manifolds intersect each other an infinite

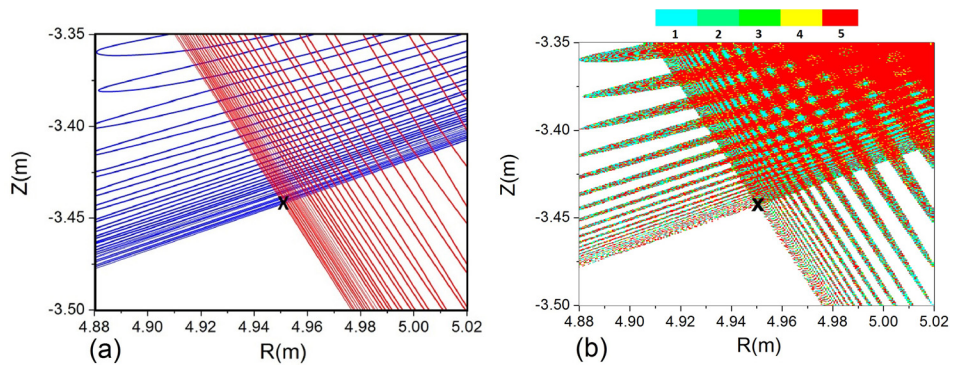

FIG. 6. Numerical calculations for system perturbed by $N = 10$ pairs of loop coils with $I_c = 70\,\text{kA}$. (a) Homoclinic tangle formed by the unstable (red) and stable (blue) manifolds from the lower X point (in black). (b) Connection lengths of the homoclinic tangle in the region near the X point (in black).

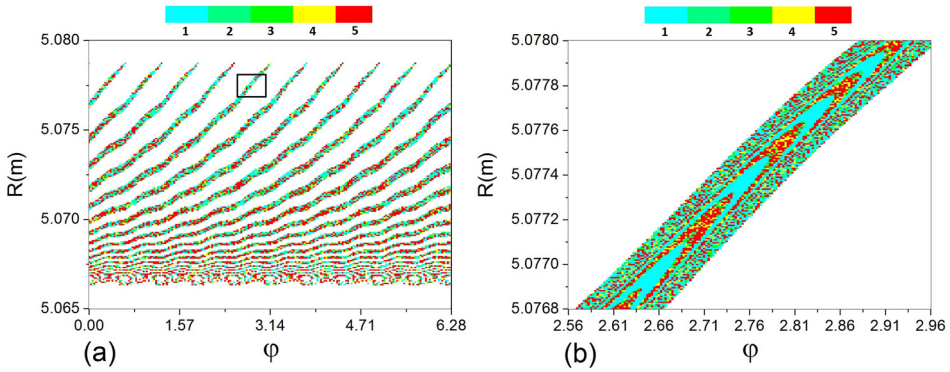

FIG. 7. (a) Magnetic footprints for the system perturbed by $N = 10$ pairs of loop coils with $I_c = 70\,\text{kA}$, showing places at the divertor plate where magnetic field lines began their trajectories, and their correspondent connection lengths. (b) Zoom at the rectangle shown in (a), emphasizing details of the structure formed by the homoclinic tangle.

number of times, forming a complex pattern known as homoclinic tangle.[5,11] Figure 6(b) shows the connection lengths of the case shown in 6(a), where the region in white color represents the initial position of field lines that take less than one toroidal turn to escape to the divertor plates. It is noticed in Figure 6(b), a structure similar to the homoclinic tangle of stable and unstable manifolds shown in Figure 6(a). This type of structure has been observed through the use of computer codes that simulate escape patterns in Ref. 19.

One can calculate the magnetic footprint which is the set of points that reaches the divertor plates. The magnetic field line is integrated backwards in φ, for initial conditions located at the divertor plate (black segment in Figure 5(b)), in a box with $5.065 \leq \text{R}_0 \leq 5.080$ and $0 \leq \varphi_0 \leq 2\pi$. Then a color map is constructed where the color indicates the connection length of the field line, and the axes, (φ, R), represent the initial position of the field lines.

The magnetic footprints of Figure 7(a) and the zoom in the rectangle in Figure 7(b) show structures created by magnetic field lines at the divertor plate (black segment in Figure 5(b)). Each color represents the connection length, namely, the number of toroidal turns required for the field line to reach the divertor plate. The manifolds of the separatrix act as boundaries for the magnetic footprints, determining their position and shape. Outside the boundaries of the separatrix one can find, in white, magnetic field lines that take less than one toroidal turn to escape to the divertor plate. We note that there are ten lobes related to the number of pairs of loops coils used in our model (see Eq. (4)). Since the structure of the homoclinic tangle is self-similar, we expect magnetic footprints to have a fractal nature.[30] Similar results were observed in sophisticated simulation codes.[20,28]

V. STICKINESS EFFECT

Chaotic field lines escape to the divertor plates, but some of them may be trapped for many toroidal turns (i.e., long connection lengths) in complex structures at the border of magnetic islands, giving rise to the so-called stickiness effect characteristic of Hamiltonian systems.[21] Since the distribution of the connection lengths directly interfere on the particle transport, determining the deposition patterns on the divertor plates,[5] it is essential to analyze the topology of sticky structures.

Figure 8 shows the connection lengths of field lines near the X point, located at the reference line, in green, of Figure 9(a), varying according to the amplitude of the current in the perturbation coils. One can notice in Figure 8(a) horizontal structures with long connection lengths (red stripes) located between regions with short connection lengths. Some of these horizontal structures (red stripes) remain intact while the current in the coils is increased. Figure 8(b) shows a zoom in the black rectangle of Figure 8(a), in order to clarify some details of the horizontal structure (red stripe) located at $-3.080 \leq \text{Z} \leq -3.062$. The red stripes in Figure 8 indicate the presence of magnetic field lines, in the diverted zone, with long connection lengths, equal or higher than 410 toroidal turns. However, the distribution of connection length values inside this red zone should be complex and determined by the reminiscent small island chains (broken and unbroken) shown in Figure 5(b). These long connection lengths reported are further discussed later on.

Figure 9(a) shows the magnetic surfaces perturbed by $N = 10$ pairs of loop coils with $I_c = 70\,\text{kA}$. The reference line in green was used to calculate the connection lengths

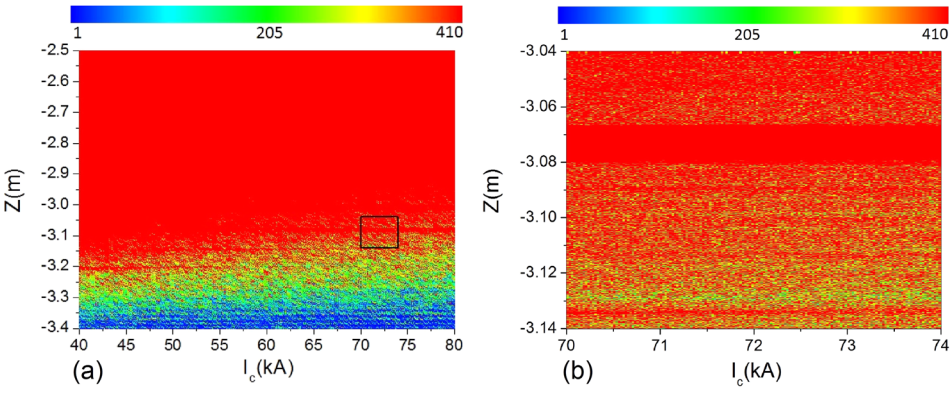

FIG. 8. (a) Color map of the connection lengths as a function of I_c and $Z(m)$, showing the existence of horizontal structures (red stripes) that remain intact for long ranges of current in the coils. The colors indicate the values of field line connection lengths; the red color represent points with long connection lengths (equal or higher than 410 toroidal turns). (b) Zoom at the black rectangle of (a), emphasizing details of a horizontal structure (red stripe) at $-3.080 \leq \text{Z} \leq -3.062$.

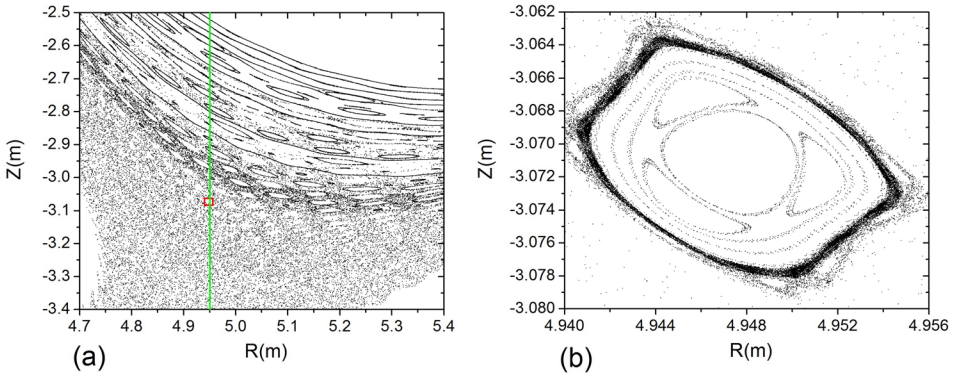

FIG. 9. (a) Magnetic surfaces perturbed by $N = 10$ pairs of loop coils with $I_c = 70\,\text{kA}$. The reference line in green was used to calculate the connection lengths distribution shown in Figure 8. (b) Zoom at the red rectangle shown in (a), emphasizing details of the island that causes the red stripe shown in Figure 8(b) at $-3.080 \leq Z \leq -3.062$.

distribution shown in Figure 8. Figure 9(b) shows a zoom of the red square of (a), constructed with the same height and position of the red stripe shown in Figure 8(b), i.e., $-3.080 \leq Z \leq -3.062$. In Figure 9(b), one can identify islands formed by field lines located on regular surfaces, and also a concentration of pixels (iterations) on the chaotic layers surrounding the island, that interfere in the field line escape.

It is worthwhile to mention that the main red stripe in the connection length, shown in Figure 8(b), represents the trapping region where the sticky island from Figure 9(b) is located, and it has, approximately, 2 cm, which, then, is larger than the typical ion Larmor radius order of millimeters.

Figure 10(a) shows a zoom at the border of the island of Figure 9(b). Figure 10(b) shows the rotation number for the field line with initial condition represented by the red dot in (a), located at the chaotic layer surrounding the island. One can notice a convergence in the rotation number for the initial 1500 toroidal turns, indicating that the field line is trapped in a resonance with rotation number $\omega = 51/250$. After that, the field line escapes entering in the chaotic sea, and its rotation number for the next toroidal turns diverges. Figures 10(c) and 10(d) show the Poincaré map of the commented field line for (c) 1500 toroidal turns and (d) 5000 toroidal turns, and the trapping effect become clearer. For the 1500 initial toroidal turns, the field line is trapped at the resonance with $\omega = 51/250$ and, after that, the field line escapes and, eventually, hits the divertor plate.

Figures 10(b)–10(d) show stickiness evidence that could be explained by the presence of cantori surrounding resonance islands. The cantori gaps are usually very small, thus a chaotic orbit inside them takes a long time before escaping to the outer chaotic sea, and a stickiness phenomenon appears.[21] One can find many stick regions in the analyzed area of Figure 8(a), although the stickiness effect analyzed in this model is a very subtle feature as the small bands in the connection length distribution, in Figure 8(a), shows. These fine structures are highly dependent on the actual perturbed magnetic field, and might be reduced in a coil set with multiple toroidal modes.

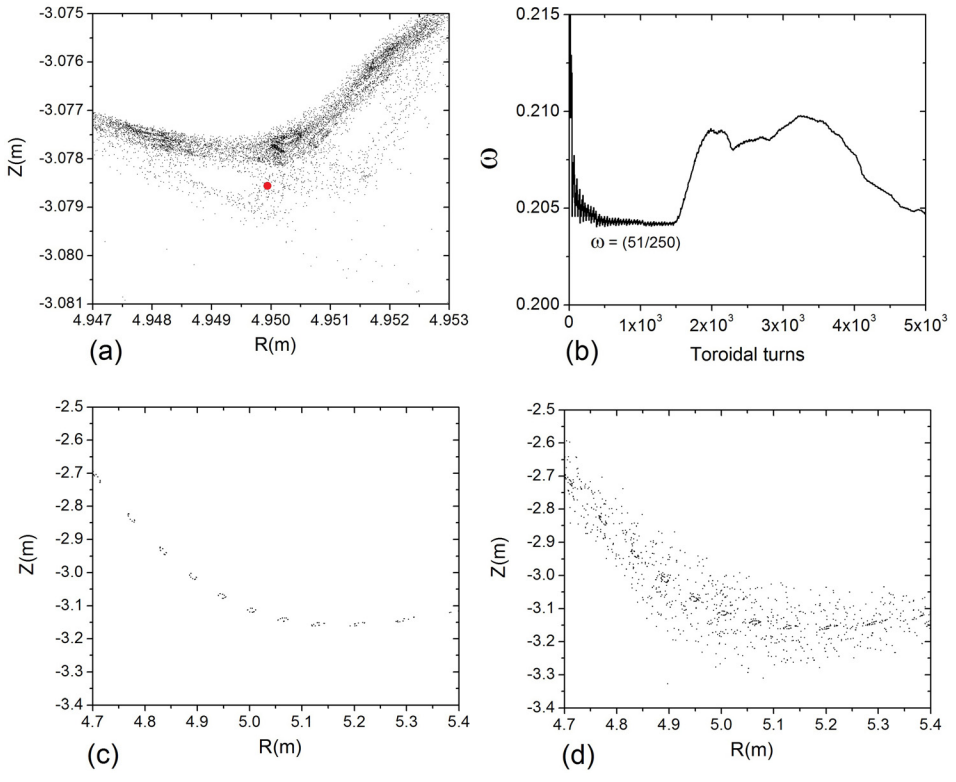

FIG. 10. (a) Zoom at the border of the island of Figure 9(b). (b) Rotation number of the initial condition represented by the red dot in (a). (c) Initial condition at the red dot in (a) iterated for 1500 toroidal turns. (d) Initial condition at the red dot in (a) iterated for 5000 toroidal turns.

VI. STICKINESS EFFECT IN A COLLISIONAL SCENARIO

Particle transport inside the plasma is not only determined by the magnetic field lines, but also by collisions. So, to estimate the stickiness effect of Sec. V, in a collisional scenario, we have to modify the field line equations to simulate how collisions divert particle center guide from the field line trajectories. It has been verified, recently, in a simple numerical model, that the manifolds of the X points still govern the particle dynamics when collisions are included.[31] To check that we add the effect of an additional noise in the system that simulates collisional diffusion of particles inside the plasma column. The effect of such noise is represented by adding a vector of random orientation to the magnetic field lines equation, at every complete toroidal turn,[32] thus, equations for the magnetic field lines become

$$\frac{dz}{d\varphi} = \frac{\partial H}{\partial p_Z} + \rho \sin(\theta_t), \quad \frac{dp_Z}{d\varphi} = -\frac{\partial H}{\partial z} + \rho \cos(\theta_t), \qquad (7)$$

where ρ is the collisional amplitude, $0 \leq \theta_t \leq 2\pi$ is a random phase, (z, p_Z) are the canonical coordinates of position and momentum, respectively, and the toroidal angle, φ, the canonical time. We choose the collisional amplitude, ρ, by analyzing the mean free path expected for a tokamak like ITER.[9]

It is well known that the divergence-free nature of the magnetic field in a tokamak, $\nabla \cdot \vec{B} = 0$, leads to modeling the magnetic field lines trough a Hamiltonian formalism, since, in this approach, the plasma particles are frozen in magnetic field lines that lie in nested magnetic surfaces. However, in our model, the collisional noise from Eq. (7) divert particle center guide from the field line trajectories; consequently, the orbit does not lie anymore in a unique magnetic surface, instead, it jumps to another magnetic surface at every complete toroidal turn, not satisfying the divergence-free of the magnetic field. Besides that, during each toroidal turn the divergence-free of the magnetic field is still satisfied.

Figure 11(a) shows the sticky island from Figure 9(b) but in a collisional regime with collisional amplitude $\rho = 1 \times 10^{-3}$. One can notice the destruction of the internal structures that used to form the island, including the structures that used to form the border of the island. Figure 11(b) shows the rotation number for the field line with initial condition represented by the red dot in 10(a), and the stickiness effect did not vanish with the addition of the collisional noise. Although, instead of being trapped for 1500 toroidal turns, the field line was trapped for 500 toroidal turns. It suggests that collisions, depending on their amplitude, do not extinct stickiness structures, but decrease their time scale of trapping. Moreover, with the inclusion of collisions as the stickiness is reduced to the number of 500 toroidal turns (see Figures 10(b) and 11(b)), a roughly estimative can be made by multiplying 500 toroidal turns for the length of the toroidal chamber, with is, approximately, 38.9 m ($2\pi R_0$). Then, the field line will perform, at least, 19468 m, more than the estimated mean free path length at ITER, until reaching the outer chaotic layer, and, eventually, the divertor plate.

Figure 12(a) shows the connection lengths of field lines near the X point, located at the reference line, in green, of Figure 9(a), in a range of $-3.40 \leq Z \leq -3.00$, for $I_c = 60$ kA, revealing two intermingled domains: laminar zones with short field line connection lengths (corresponding to the low toroidal peaks), and zones with long connection lengths, equal or longer than 410 toroidal turns (corresponding to high toroidal peaks/plateaus). According to Refs. 9 and 19, resonant magnetic perturbations destroy the magnetic surfaces near the hyperbolic points and lead to chaotic field lines diffusion, identified by field lines with long connection lengths. Complementary, intervals of short connection lengths are due to the field lines which do not mix with the chaotic interior, but connect on short distances to the divertor targets.[19] Here, we conjecture that, in Figure 12(a), the short connection lengths reveal laminar regions, while some of the long connection lengths, identified by the plateaus, maybe caused by stickiness inside the diverted region.

In order to clarify the low peaks and plateaus from Figure 12(a), and understand their dependence on the coils current, we generate Figure 12(b), where we calculate, for a large number of initial conditions located at the green reference line of Figure 9(a), in the interval $-3.40 \leq Z \leq -3.00$, the escape time statistics (ETS)[35]

$$\rho(\tau) = \frac{N_{escape}}{N_{total}}, \qquad (8)$$

where N_{escape} is the number of initial field lines that reach the divertor plates with toroidal turns $n \geq \tau$ and N_{total} is the total number of initial field lines that actually reach the divertor plates. As a matter of fact, Eq. (8) represents a cumulative

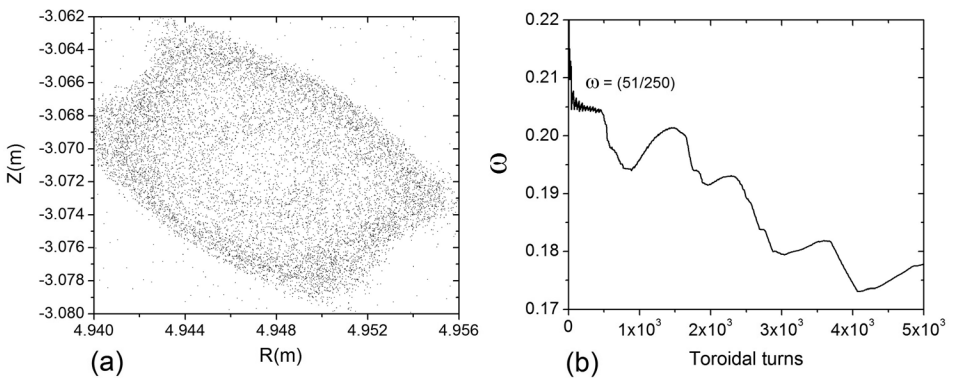

FIG. 11. (a) Sticky island from Figure 9(b) in a collisional regime with $\rho = 1 \times 10^{-3}$. (b) Rotation number of the initial condition represented by the red dot in Figure 10(a) in a collisional regime.

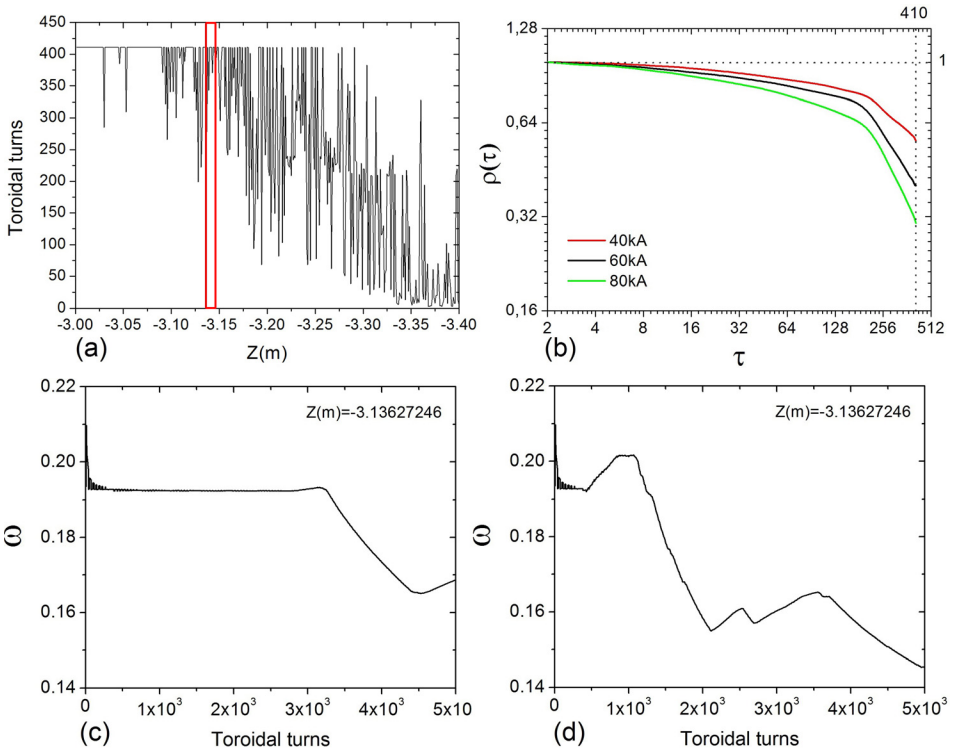

FIG. 12. (a) Connection lengths as a function of $Z(m)$, for $I_c = 60\,\text{kA}$. Red rectangle indicates the stickiness region analyzed in (c). (b) Escape time statistic, $\rho(\tau)$, as a function of the toroidal turns, for a large number of initial conditions located at the reference line, in green, of Figure 9(a), in a range of $-3.40 \leq Z \leq -3.00$, displayed as a logarithmical base two plot. The vertical dotted line indicates the integration limit of the considered toroidal turns, $\tau = 410$, and the horizontal dotted line indicates $\rho = 1$. (c) Rotation number for one initial condition at the border of a sticky island, forming the plateau inside the red rectangle in (a), at $Z = -3.13627246$. (d) Rotation number for the same initial condition at (c), but in a collisional regime with amplitude $\rho = 1 \times 10^{-3}$.

distribution function that decreases from two toroidal turns, $\rho(2) = 1$, to $\tau = 410$ toroidal turns. We displayed the results as a logarithmical base two plot and we showed the ETS for three different currents in the coils. The vertical dotted line indicates the integration limit of the considered toroidal turns, $\tau = 410$, and the horizontal dotted line indicates $\rho = 1$.

For $\tau \leq 128$ toroidal turns, the ETS related to $I_c = 40\,\text{kA}$, $I_c = 60\,\text{kA}$, and $I_c = 80\,\text{kA}$, have a quasi-linear decay (smoothly curved). It can be confirmed through the layers formed by the connection length distribution, in Figure 8(a), for toroidal turns between 1 (dark blue) and 128 (light green). Then, initially, we conclude that the chaotic layers of these three cases, for $\tau \leq 128$, are quite similar. Furthermore, for long toroidal turns, $\tau > 256$, the decay, for the three cases, is drastic, indicating the presence of some kind of trapping in the diverted zone.

Next, to understand one of the origins of the drastic decay of Figure 12(b), we show in Figure 12(c) the rotation number for a field line with initial condition located at the reference line, in green, of Figure 9(a), at $Z = -3.13627246$, located at the chaotic layer surrounding a sticky island chain, forming the plateau inside the red rectangle in Figure 12(a). One can notice a convergence in the rotation number for the initial 3000 toroidal turns, indicating that the field line is trapped in a resonance with rotation number $\omega = 24/125$. After that, the field line escapes entering in the chaotic sea, and its rotation number for the next toroidal turns diverges. Figure 12(c) evidences a stickiness effect remaining island chain, which contributes to the formation of the plateaus of Figure 12(a), and the drastic decay of Figure 12(b). This trapping is similar to the stickiness around island chains identified in the tokamak plasma edges perturbed by resonant external coils[26] and in other symplectic maps.[33–35] In fact, according to Refs. 33 and 34, the intensity of the stickiness around the reminiscent small magnetic islands depends on the structure of their homoclinic tangle.

Figure 12(d) shows the rotation number for the same case of Figure 12(c), but in a collisional regime with collisional amplitude $\rho = 1 \times 10^{-3}$, and the observed trapping did not vanish with the addition of the collisional noise. Although, instead of being trapped for 3000 toroidal turns, the field line was trapped for 500 toroidal turns. Once again, it suggests that collisions, depending on their amplitude, do not extinct trapping structures, but decrease their time scale.

More sticky island chains can be found in Figure 12(a) influencing the drastic decay of Figure 12(b), and the effect of all sticky islands in the diverted region increases the number of toroidal turns of magnetic field lines until them reach the divertor plates. But, once again, the presence of sticky islands emphasized here is very subtle and might be reduced in a scenario with a coil set with multiple toroidal modes.

VII. CONCLUSIONS

The Hamiltonian model presented in this work is capable of reproducing magnetic surfaces expected in tokamak equilibria with divertor. An external perturbation, analogous to the perturbation of the C-coils installed at the tokamak DIII-D and those that will be installed at ITER, was added to study qualitatively the dynamical characteristics of the magnetic field lines in a chaotic divertor layer. By tracing the manifolds, we showed the influence of the homoclinic tangle on the deposition patterns of field lines in the divertor plates, agreeing qualitatively with results obtained with sophisticated computer codes. The evidences of stickiness effect, around magnetic island chains embedded in the diverted region were analyzed, indicating that this effect survives for

long ranges of current in the perturbation coils, trapping magnetic field lines for many toroidal turns. A random noise was added to the field line equation to simulate collisions between the plasma particles, and the stickiness evidences did not vanish under the presence of such collisions. However, the time scale of the trapping decreased when compared to the case without collisions. The reported results indicate that the trapping caused by remaining magnetic islands may affect the transport in present tokamaks.

ACKNOWLEDGMENTS

The authors would like to thank Dr. P. J. Morrison, Dr. T. Kroetz, and Dr. C. Vieira Abud for useful comments, and the following Brazilian scientific agencies for the financial support: CAPES, The National Council for Scientific and Technological Development (CNPq), Grant 211630/2013-6, and São Paulo Research Foundation (FAPESP), Grants 2010/13162-0, 2013/03401-6, and 2011/19269-11. The views and opinions expressed herein do not necessarily reflect those of the ITER Organization.

APPENDIX: UNPERTURBED HAMILTONIAN EQUATION

In this appendix, we present the unperturbed Hamiltonian equation, in (R, Z, φ) coordinates (see Figure 1), introduced in Ref. 10, and used in the present article. Accordingly, the magnetic field line equations are

$$\frac{1}{R}\left(\frac{dZ}{d\varphi}\right) = \frac{B_z}{B_\varphi}, \quad \frac{1}{R}\left(\frac{dR}{d\varphi}\right) = \frac{B_R}{B_\varphi}. \tag{A1}$$

The magnetic field $\vec{B}$ can be expressed by the vector potential $\vec{A}(R, Z, \varphi) = (A_R, A_Z, A_\varphi)$, so that $\vec{B} = \nabla \times \vec{A}$. Therefore, the component of the magnetic field can be written as

$$\begin{aligned} B_R &= \frac{1}{R}\left(\frac{\partial A_Z}{\partial \varphi}\right) - \left(\frac{\partial A_\varphi}{\partial Z}\right), \\ B_\varphi &= -\frac{\partial A_Z}{\partial R}, \\ B_Z &= \frac{1}{R}\left(\frac{\partial R A_\varphi}{\partial R}\right). \end{aligned} \tag{A2}$$

We introduce canonical variables (z, p_Z) associated with the geometric coordinates (R, Z) and the magnetic field, according to[10]

$$z = \frac{Z}{R_0}, \quad p_Z = \frac{1}{B_0 R_0}\int_{R_0}^{R} B_\varphi dR. \tag{A3}$$

The toroidal magnetic field is expressed by $B_\varphi(R) = B_0 R_0/R$, then $Z = R_0 z$ and $R = R_0 e^{p_z}$, and the equations for the field lines can be transformed to Hamiltonian form

$$\frac{dz}{d\varphi} = \frac{\partial H}{\partial p_Z}, \quad \frac{dp_Z}{d\varphi} = -\frac{\partial H}{\partial z}. \tag{A4}$$

The variables (z, p_Z) are the canonical coordinates of position and momentum, respectively, and the toroidal angle, φ, the canonical time.

The vector potential for each current loop is given by[10]

$$A_\varphi(R, Z) = \sum_{j=1}^{5} \frac{\mu_0 I_j}{\pi k_j}\sqrt{\frac{R_0}{R}}\left[\left(1 - \frac{k_j^2}{2}\right)K(k_j) - E(k_j)\right], \tag{A5}$$

where $K(k_j)$ and $E(k_j)$ are the complete elliptic integrals with module

$$k_j^2 = \frac{4R_0 R}{(R + R_0)^2 + (Z - Z_j)^2}, \quad j = 1, ..., 5. \tag{A6}$$

For a tokamak with large aspect ratio, $(R_0/a \gg 1)$, the unperturbed Hamiltonian, $H_0(z, p_Z) = -(RA_\varphi(R, Z))/(B_0 R_0^2)$, can be approximated to

$$\begin{aligned} H_0(z, p_Z) = \frac{-1}{R_0}\sum_{j=1}^{5}\frac{\mu_0 I_j}{4\pi B_0}\Bigg(\ln\Bigg(64\Bigg(\Bigg[\left(\frac{R}{R_0} - \frac{R_j}{R_0}\right)^2 \\ + \left(\frac{Z}{R_0} - \frac{Z_j}{R_0}\right)^2\Bigg]^{-1}\Bigg)\Bigg) - 4\Bigg). \end{aligned} \tag{A7}$$

[1]W. M. Stacey, Jr., *Fusion Plasma Analysis* (John Wiley & Sons, New York, 1981).
[2]ITER Physics Expert Group on Divertor, Nucl. Fusion **39**, 2391 (1999).
[3]F. Wagner, G. Becker, K. Behringer, D. Campbell, A. Eberhagen, W. Engelhardt, G. Fussmann, O. Gehre, J. Gernhardt, G. V. Gierke, G. Haas, M. Huang, F. Karger, M. Keilhacker, O. Klüber, M. Kornherr, K. Lackner, G. Lisitano, G. G. Lister, H. M. Mayer, D. Meisel, E. R. Müller, H. Murmann, H. Niedermeyer, W. Poschenrieder, H. Rapp, H. Röhr, F. Schneider, G. Siller, E. Speth, A. Stäbler, K. H. Steuer, G. Venus, O. Vollmer, and Z. Yü, Phys. Rev. Lett. **49**(19), 1408 (1982).
[4]M. Kikuchi, K. Lackner, and M. Tran, *Fusion Physics* (IAEA, Vienna, 2012).
[5]T. E. Evans, R. A. Moyer, and P. Monat, Phys. Plasmas **9**, 4957 (2002).
[6]A. Wingen, T. E. Evans, and K. H. Spatschek, Nucl. Fusion **49**, 055027 (2009).
[7]T. A. Casper, W. H. Meyer, L. D. Pearlstein, and A. Portone, Fusion Eng. Des. **83**, 552 (2008).
[8]M. Brix, N. C. Hawkes, A. Boboc, V. Drozdov, S. E. Sharapov, and JET-EFDA Contributors, Rev. Sci. Instrum. **79**, 10F325 (2008).
[9]T. Kroetz, C. G. L. Martins, M. Roberto, and I. L. Caldas, J. Plasma Phys. **79**(05), 751 (2013).
[10]S. S. Abdullaev, K. H. Finken, M. Jakubowski, and M. Lehnen, Nucl. Fusion **46**, S113 (2006).
[11]E. C. da Silva, I. L. Caldas, R. L. Viana, and M. A. F. Sanjuan, Phys. Plasmas **9**(12), 4917 (2002).
[12]A. H. Boozer and A. B. Rechester, Phys. Fluids **21**, 682 (1978).
[13]N. Pomphrey and A. Reiman, Phys. Fluids B **4**, 938 (1992).
[14]H. Ali, A. Punjabi, A. Boozer, and T. E. Evans, Phys. Plasmas **11**, 1908 (2004).
[15]H. Ali, A. Punjabi, and A. Boozer, J. Plasma Phys **75**, 303 (2008).
[16]U. Daybelge and C. Yarim, J. Nucl. Mater. **266–269**, 809 (1999).
[17]A. Reiman, Phys. Plasmas **3**, 906 (1996).
[18]A. Foussat, P. Libeyre, N. Mitchell, Y. Gribov, C. T. J. Jong, D. Bessette, R. Gallix, P. Bauer, and A. Sahu, IEEE Trans. Appl. Supercond. **20**(3), 402 (2010).
[19]O. Schmitz *et al.*, Plasma Phys. Controlled Fusion **50**, 124029 (2008).
[20]A. Wingen, T. E. Evans, and K. H. Spatschek, Phys. Plasmas **16**, 042504 (2009).
[21]G. Contopoulos and M. Harsoula, Int. J. Bifurcation Chaos **20**, 2005 (2010).
[22]G. Janeschitz, The Status of ITER: The ITER Design Review, paper presented at APS–DPP Town Meeting on ITER Design Review, Orlando, FL, 2007.
[23]K. H. Finken, S. S. Abdullaev, T. Eich, D. W. Faulconer, M. Kobayashi, R. Koch, G. Mank, and A. Rogister, Nucl. Fusion **41**, 503 (2001).
[24]Ph. Ghendrih, A. Grosman, and H. Capes, Plasma Phys. Controlled Fusion **38**, 1653 (1996).

[25]M. Z. Tokar, Phys. Plasmas **6**, 2808 (1999).
[26]T. Kroetz, M. Roberto, E. C. da Silva, I. L. Caldas, and R. L. Viana, Phys. Plasmas **15**, 092310 (2008).
[27]R. K. W. Roeder, B. I. Rapoport, and T. E. Evans, Phys. Plasmas **10**, 3796 (2003).
[28]M. W. Jakubowski, T. E. Evans, M. E. Fenstermacher, M. Groth, C. J. Lasnier, A. W. Leonard, O. Schmitz, J. G. Watkins, T. Eich, W. Fundamenski, R. A. Moyer, R. C. Wolf, L. B. Baylor, J. A. Boedo, K. H. Burrell, H. Frerichs, J. S. de Grassie, P. Gohil, I. Joseph, S. Mordijck, M. Lehnen, C. C. Petty, R. I. Pinsker, D. Reiter, T. L. Rhodes, U. Samm, M. J. Schaffer, P. B. Snyder, H. Stoschus, T. Osborne, B. Unterberg, E. Unterberg, and W. P. West, Nucl. Fusion **49**(9), 095013 (2009).
[29]M. W. Jakubowski, S. S. Abdullaev, K. H. Finken, M. Lehnen, and the TEXTOR Team, J. Nucl. Mater. **176**, 337–339 (2005).
[30]R. L. Viana, E. C. Da Silva, T. Kroetz, I. L. Caldas, M. Roberto, and M. A. F. Sanjuán, Philos. Trans. R. Soc. A **369**, 371 (2011).
[31]A. B. Schelin, I. L. Caldas, R. L. Viana, and M. S. Benkadda, Phys. Lett. A **376**, 24 (2011).
[32]P. Beaufume, M. A. Dubois, and M. S. Benkadda, Phys. Lett. A **147**, 87 (1990).
[33]J. D. Szezech, I. L. Caldas, R. L. Viana, and P. J. Morrison, Chaos **19**, 043108 (2009).
[34]J. D. Szezech, I. L. Caldas, S. R. Lopes, P. J. Morrison, and R. L. Viana, Phys. Rev. E **86**, 036206 (2012).
[35]C. Vieira Abud and I. L. Caldas, Nucl. Fusion **54**(6), 064010 (2014).